Mathematical Modeling of K-Ras Nanocluster Formation on the Plasma Membrane

Tianhai Tian,[†] Sarah J. Plowman,[‡] Robert G. Parton,[§] Yoel Kloog,[¶] and John F. Hancock[‡*]
[†]Department of Mathematics, University of Glasgow, Glasgow, United Kingdom; [‡]Department of Integrative Biology and Pharmacology, University of Texas Health Science Center at Houston, Houston, Texas; [§]Institute for Molecular Bioscience, University of Queensland, Brisbane, Queensland, Australia; and [¶]Department of Neurobiochemistry, The George S. Wise Faculty of Life Sciences, Tel Aviv University, Tel Aviv, Israel

ABSTRACT K-Ras functions as a critical node in the mitogen-activated protein kinase (MAPK) pathway that regulates key cellular functions including proliferation, differentiation, and apoptosis. Following growth factor receptor activation K-Ras.GTP forms nanoclusters on the plasma membrane through interaction with the scaffold protein galectin-3. The generation of nanoclusters is essential for high fidelity signal transduction via the MAPK pathway. To explore the mechanisms underlying K-Ras.GTP nanocluster formation, we developed a mathematical model of K-Ras-galectin-3 interactions. We designed a computational method to calculate protein collision rates based on experimentally determined protein diffusion rates and diffusion mechanisms and used a genetic algorithm to search the values of key model parameters. The optimal estimated model parameters were validated using experimental data. The resulting model accurately replicates critical features of K-Ras nanoclustering, including a fixed ratio of clustered K-Ras.GTP to monomeric K-Ras.GTP that is independent of the concentration of K-Ras.GTP. The model reproduces experimental results showing that the cytosolic level of galectin-3 determines the magnitude of the K-Ras.GTP clustered fraction and illustrates that nanoclustering is regulated by key nonequilibrium processes. Our kinetic model identifies a potential biophysical mechanism for K-Ras nanoclustering and suggests general principles that may be relevant for other plasma-membrane-localized proteins.

INTRODUCTION

The mitogen-activated protein kinase (MAPK) pathway transmits signals from activated growth factor receptors at the cell surface to transcription factors in the nucleus to regulate cellular functions including proliferation, differentiation, and apoptosis (1,2). The MAPK module comprises a set of three protein kinases, Raf, MEK, and ERK, which have highly conserved molecular architecture and act sequentially. The MAPK pathway is an ideal model system for mathematical modeling because the regulatory mechanisms operating on the pathway are well characterized, at least in terms of the molecular components. Over the last decade, MAPK signaling has been used repeatedly as a testable paradigm for pioneering computational systems biology (3–5). Although the principal hierarchy of the signaling pathway and its activation sequence are well established, recent data have yielded additional information on critical protein-protein interactions, regulatory loops, and spatiotemporal organization. Recent advances in the molecular understanding of MAPK signaling pose new challenges for mathematical modeling strategies (6).

Ras GTPases are guanine-nucleotide-binding proteins that act as molecular switches on the inner leaflet of the plasma membrane. Ras proteins function as a critical node between growth factor receptors and the MAPK pathway. In response to growth factor receptor activation, Ras proteins are activated by guanine nucleotide exchange factors. In the active GTP-bound state, Ras.GTP recruits downstream effectors from the cytosol to the plasma membrane. In the case of the MAPK module, Ras.GTP provides signal input by recruiting Raf to the plasma membrane, where the kinase is activated, in turn triggering activation of MEK and ERK.

Differences in the strength and/or duration of a growth factor signal induce distinct cellular outcomes. Therefore to maintain tissue homeostasis, mechanisms are required to convert the strength of a growth factor signal into the appropriate level of intracellular signal with high fidelity. Recent experimental studies show that K-Ras exhibits a tightly regulated nonrandom distribution on the inner leaflet of the plasma membrane (7–10). Approximately 40% of K-Ras proteins are organized into nanoclusters of around seven proteins with radii of ~9 nm. The 60% of nonclustered K-Ras proteins remaining are arrayed as monomers (8). We have recently shown that K-Ras nanoclusters, but not K-Ras monomers, recruit and activate Raf and therefore act as signaling platforms (5,11). Each nanocluster operates as a transient low-threshold digital switch that dumps a fixed quantum of ERKpp into the cytosol (5). Thus, K-Ras nanoclusters allow the plasma membrane to operate as an analog-digital-analog signal converter that transduces the strength of an epidermal growth factor (EGF) signal into a corresponding level of cytosolic activated ERKpp with high fidelity (5,12). Central to this signal transmission mechanism is the fixed ratio of K-Ras.GTP proteins in nanoclusters to K-Ras.GTP

Submitted September 9, 2009, and accepted for publication April 22, 2010.

*Correspondence: John.F.Hancock@uth.tmc.edu

Editor: Amitabha Chattopadhyay.

0006-3495/10/07/0534/10 $2.00

doi: 10.1016/j.bpj.2010.04.055

proteins diffusing as monomers, which remains constant over a multilog range of K-Ras.GTP expression levels (8). The fixed K-Ras.GTP clustered fraction results in a linear relationship between the number of K-Ras.GTP nanoclusters on the plasma membrane and the stimulating EGF concentration (5,8).

How the fixed K-Ras clustered fraction is achieved has yet to be elucidated. However, we have recently shown that the formation of the K-Ras.GTP nanocluster is dependent upon the recruitment of the β-galactoside-binding protein galectin-3 (Gal3) from the cytosol to the plasma membrane, where it forms an integral component of the nanocluster (13). The interaction between Gal3 and K-Ras is GTP- and farnesyl-dependent and requires a putative prenyl-binding pocket on Gal3 (14). An important question arising from these data is, how does Gal3 contribute to K-Ras.GTP nanocluster organization? Gal3 contains a C-terminal carbohydrate-recognition-binding domain and an N-terminal proline-and-glycine-rich domain (15). Gal3 can form higher-order oligomers such as pentamers and hexamers through homotypic N-terminal interactions (16,17). The oligomerization of secreted Gal3 is implicated in regulating growth factor receptor activation and immune cell function (18–20). Therefore, oligomerization of cytosolic Gal3 may also be required for intracellular function.

Taken together, these data raise a number of complex biological questions relating to plasma membrane nanoscale organization and K-Ras signal transduction. Although it is recognized that protein diffusion and collision on the plasma membrane are stochastic processes (10,23–25), stochastic models have been restricted to the study of the dynamics of very simple systems due to the huge computational time involved (21,22,26–28). To model biochemical reaction systems, or protein diffusion with multiple complex species, deterministic approaches in terms of ordinary differential equations are still the dominant method (29–31). In addition, the availability of adequate experimental data for determining kinetic rates and protein concentrations represents a significant challenge for this type of computational modeling work. For example, the number of Gal3 molecules in the cytosol for recruitment by K-Ras.GTP is not known, because Gal3 distributes into a number of different pools in the cell. Although a number of strategies have been developed for estimating parameters from experimental observations, the very real possibility exists that there are multiple different parameter sets that can realize the same experimental observation, but that reflect very different underlying mechanisms (26–28). Here, we develop a mathematical model of K-Ras nanocluster formation on the plasma membrane based on experimental discoveries to investigate the critical function of Gal3 in K-Ras.GTP nanocluster formation and address these challenges in computational biology by using a genetic algorithm to search for the values of key parameters in the mathematical model.

METHODS

A computational model for K-Ras.GTP nanocluster formation

Recently, we showed that Gal3 is recruited to plasma membrane nanoclusters by K-Ras.GTP and operates as a scaffolding protein for the signaling platform (13). To investigate how Gal3 interaction might regulate K-Ras.GTP nanocluster formation, we developed a mathematical model to simulate the diffusion and collision of K-Ras proteins on the plasma membrane (Fig. 1). The model system contains two species of protein: activated K-Ras (K-Ras.GTP) and its specific binding partner Gal3. K-Ras proteins are randomly distributed on the plasma membrane, whereas Gal3 localizes to the cytosol but can be recruited by K-Ras.GTP to form K-Ras.GTP-Gal3 (Ras-Gal3) complexes (Fig. 1, *reaction 1*). These Ras-Gal3 complexes diffuse randomly on the plasma membrane and bind to each other to form dimers through the extended N-terminal domain of Gal3 (17) (Fig. 1, *reaction 2*). A Ras-Gal3 dimer may disassociate or bind to another Ras-Gal3 complex to form a trimer. This binding process can continue until a pentamer of Ras-Gal3 complexes is formed (Fig. 1, *reactions 3–5*). Although K-Ras.GTP can bind to Ras-Gal3 complexes to form the dimeric, trimeric, or tetrameric (Ras)i-(Ras-Gal)j complexes by random diffusion, the probabilities of these binding reactions are relatively very small compared to the fast formation of Ras-Gal3 pentamers. For simplicity, these binding reactions are therefore not included in the model.

A pentamer of Ras-Gal3 complexes is regarded as the basic core structure of a nanocluster. K-Ras.GTP and Ras-Gal3 complexes can still bind to the Ras-Gal3 pentamer by random diffusion and collision with a consequent increase in the number of Ras proteins in the nanocluster (Fig. 1, *reactions 6* and *7*). A Ras nanocluster is thus defined as any protein complex containing five or more Ras proteins. When a nanocluster disassembles, it separates completely into individual Ras proteins and/or Ras-Gal3 complexes (Fig. 1, *reaction 8*). For a nanocluster with more than five Ras proteins, additional Ras proteins attached to the Ras-Gal3 pentamer can disassociate from the pentameric nanocluster (Fig. 1, *reactions 6* and *7*). In addition, a Ras-Gal3 complex can disassociate from a nanocluster as separate Ras and Gal3 proteins (Fig. 1, *reaction 9*). If this Ras-Gal3 complex is one of the complexes in the core pentamer of a nanocluster, this disassociation can lead to the disassembly of the nanocluster (Fig. 1, *reaction 10*). All biochemical reactions of the system are listed below.

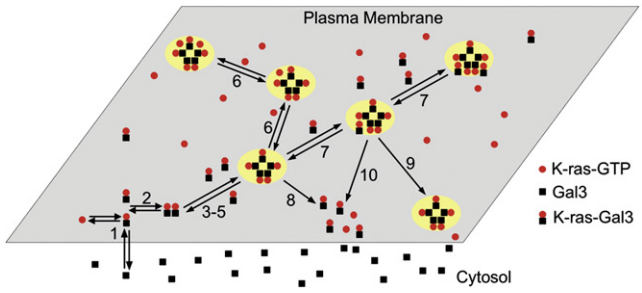

FIGURE 1 Model of K-Ras protein diffusion and collision to form nanoclusters. In this model, K-Ras.GTP diffuses randomly on the plasma membrane. Gal3 is confined to the cytosol unless recruited to the plasma membrane by K-Ras.GTP (*1*). Assembly of K-Ras nanoclusters proceeds by collision of Ras-Gal3 complexes to form dimers (*2*) and subsequently pentamers (*3-5*). Formation of nanoclusters with a higher stochiometry is possible by collision of additional K-Ras.GTP proteins or Ras-Gal3 complexes with Ras-Gal3 pentamers (*6,7*). Disassembly of a nanocluster can proceed either by complete disaggregation into the constituent K-Ras.GTP monomers and Ras-Gal3 complexes (*8,10*) or by loss of single K-Ras.GTP or Ras-Gal3 complexes (*6,7,9*).

$$\mathrm{Ras} + \mathrm{Gal3} \underset{d_1}{\overset{a_1}{\rightleftarrows}} \mathrm{Ras-Gal3} \tag{1}$$

$$\mathrm{Ras-Gal3} + \mathrm{Ras-Gal3} \underset{d_2}{\overset{a_2}{\rightleftarrows}} (\mathrm{Ras-Gal3})2 \tag{2}$$

$$\mathrm{Ras-Gal3} + (\mathrm{Ras-Gal3})2 \underset{d_3}{\overset{a_3}{\rightleftarrows}} (\mathrm{Ras-Gal3})3 \tag{3}$$

$$\mathrm{Ras-Gal3} + (\mathrm{Ras-Gal3})3 \underset{d_4}{\overset{a_4}{\rightleftarrows}} (\mathrm{Ras-Gal3})4 \tag{4}$$

$$\mathrm{Ras-Gal3} + (\mathrm{Ras-Gal3})4 \underset{d_5}{\overset{a_5}{\rightleftarrows}} (\mathrm{Ras-Gal3})5 \tag{5}$$

$$(\mathrm{Ras-Gal3})i - (\mathrm{Ras})j + \mathrm{Ras} \underset{d_{6ij}}{\overset{a_6}{\rightleftarrows}} (\mathrm{Ras-Gal})i - (\mathrm{Ras})(j+1) \tag{6}$$

$$(\mathrm{Ras-Gal3})i - (\mathrm{Ras})j + \mathrm{Ras} - \mathrm{Gal3} \underset{d_{7ij}}{\overset{a_7}{\rightleftarrows}} (\mathrm{Ras-Gal3})(i+1) - (\mathrm{Ras})j \tag{7}$$

$$(\mathrm{Ras-Gal3})\mathrm{i} - (\mathrm{Ras})\mathrm{j} \overset{d_8}{\rightarrow} i \times (\mathrm{Ras-Gal3}) + j \times (\mathrm{Ras}) \tag{8}$$

$$(\mathrm{Ras-Gal3})i - (\mathrm{Ras})j \overset{d_{9i}}{\rightarrow} (\mathrm{Ras-Gal3})(i-1) - (\mathrm{Ras})j + \mathrm{Ras} + \mathrm{Gal3}(\mathrm{i} \geq 6) \tag{9}$$

$$(\mathrm{Ras-Gal3})i - (\mathrm{Ras})j \overset{d_{10}}{\rightarrow} (i-1) \times (\mathrm{Ras-Gal3}) + (j+1) \times (\mathrm{Ras}) + \mathrm{Gal3}. \tag{10}$$

It is assumed that binding rates, a_3, a_4, and a_5, are equal to a_2, because these binding reactions are all based on the same properties of the extended N-terminal domain of Gal3. The disassociation rates d_8, d_{6ij} ($j \times d_8$), and d_{7ij} ($(i-5) \times d_8$) are based on the averaged lifetime of a K-Ras protein in a nanocluster (9,10); in addition, $d_{9i} = (i\text{-}5) \times d_9$. All other rates ($a_1$, d_1, a_2, d_2, a_6, a_7, d_9, and d_{10}) were estimated using a genetic algorithm. Since the averaged number of K-Ras.GTP in a nanocluster is 7 and the minimal number of Ras protein in a nanocluster is 5, we assume for simplicity that the maximal number of Ras proteins in a nanocluster is 10.

This system contains 136 reactions and 27 complex species. Therefore, due to the huge computational time that would be required, it is not practical to develop a spatial stochastic model to investigate the collision of K-Ras and Gal3 on the plasma membrane. The recruitment and binding reactions are assumed to occur in a homogeneous environment and molecular spatial heterogeneity is not considered. We developed a deterministic model (Supporting Material) in terms of a system of 27 ordinary differential equations based on the reactions listed above. The deterministic model was simulated using the Runge-Kutta method for solving stiff differential equations (ode23s in MATLAB).

Method for calculation of collision rates

To further develop the mathematical model, we designed a numerical method to estimate protein collision rates on the plasma membrane. The method, which is based on experimentally determined protein diffusion mechanisms, has the following assumptions.

1. The diffusion rate of K-Ras.GTP on the plasma membrane is 1 $\mu m^2/s$ (24).
2. It is assumed that a Ras-Gal3 complex has the same diffusion rate, given the weak dependence of diffusion rate on molecular diameter (25).
3. When a nanocluster forms, it becomes immobile on the plasma membrane (10) and its diffusion rate is therefore zero.
4. It is assumed that the area of a Ras protein is 2 nm^2, corresponding to a radius of 0.8 nm.
5. We assume that Gal3 is the same size as a Ras protein, and thus that the radius of a Ras-Gal3 complex is 1.6 nm. The mean radius of a K-Ras nanocluster is 9 nm (8).
6. The maximal number of K-Ras.GTP proteins that can be generated on the plasma membrane of a BHK cell is 774,000 (5).
7. Since ~42% of K-Ras proteins are localized in nanoclusters at equilibrium (8), we use a K-Ras.GTP number of 448,920 (774,000 × 0.58) to calculate the collision rates of the Ras-Gal3 complex. This calculation gives the maximum number of K-Ras.GTP nanoclusters as 46,440 (5).
8. The maximal area of the square simulation surface is 1256.44 μm^2 (the surface area of a cell with radius 10 μm).
9. The lateral diffusion of Brownian particles in a medium characterized by a diffusion coefficient D is described by the cumulative distribution function of the square displacements r^2, given by

$$P(r^2, \Delta t) = 1 - C\exp\left(-\frac{r^2}{r_0^2(\Delta t)}\right), \tag{11}$$

where C is a normalized factor and $C = 1$ in this work. Here, $P(r^2, \Delta t)$ is the probability that the Brownian particle starting at the origin will be found within a circle of radius r at the time lag, Δt (23,24). Equation 11 is valid when Δt is very short, for example, when $\Delta t = 5 \sim 60$ ms (24). K-Ras protein diffusion on the plasma membrane satisfies the mean-square displacement of $r_0^2(\Delta t) = 4D\Delta t$ (23,24,32). Previous work has validated Eq. 11 using the theory of diffusion-limited reactions in two dimensions (33). It is clear that the return probability for a random walker in two dimensions (as the time lag Δt becomes large) is 1.

Assuming that two species of proteins with molecular numbers N_1 and N_2, diffusion rates D_1 and D_2, and radii r_1 and r_2 are randomly distributed on a square surface (with length L) whose area is equal to that of the cell surface, we can formulate the following method to calculate the protein collision rate on the plasma membrane.

1. Generate two random samples of $U(0,L)$, which is the uniformly distributed random variable on interval (0, L), as (x_i, y_i), to determine the location of each protein in the square with length L. To avoid any initial protein collision, the distance between any two proteins should be larger than the sum of their radius.
2. For a given very small Δt, calculate the new position of each protein based on the lateral diffusion of Brownian particles (Eq. 11). Two random samples (s_1, s_2) are generated from the uniformly distributed random variable $U(0,1)$ to determine the moving distance, r, and direction, θ, of a protein over Δt based on

$$s_1 = P(r^2, \Delta t), \quad \theta = 2\pi s_2.$$

The protein will then move from the previous position (x_{i0}, y_{i0}) to new position (x_{i1}, y_{i1}), determined by

$$x_{i1} = x_{i0} + r\cos(\theta),\ y_{i1} = y_{i0} + r\sin(\theta).$$

If the new position is outside the square, a position inside the square will be determined according to periodic boundary conditions.

3. Calculate the distance from each protein of the first species to every protein of the second species and count the number of protein collisions, M, if the distance between them is less than the sum of the radii of the corresponding proteins.

4. Calculate the collision rate by

$$k = \frac{MS}{N_1 N_2 \Delta t}.$$

If it is a dimeric reaction, the collision rate is

$$k = \frac{2MS}{N(N-1)\Delta t}.$$

where S is the volume of the reactant area. It is assumed that the surface area of a cell is the unit 1.

Genetic algorithm for estimating model parameters

The genetic algorithm is an effective technique to find approximate solutions for complex search problems. We used a MATLAB toolbox to estimate nine model parameters including eight kinetic rates and the number of Gal3 molecules (34). The fitness function of a dynamic model can be defined either as the difference between time-scaled data or the difference between equilibrium data (35). In our work, the estimation error is defined as the difference between simulation results and two experimental observations: the constant fraction (~42%) of K-Ras.GTP in nanoclusters over a wide range of K-Ras.GTP numbers (8) and the averaged number (~7) of K-Ras.GTP/nanocluster (8). The widely used mean-square relative error was used to measure the model estimation error, defined by

$$\text{Error} = \sum_{i=1}^{10}\left[\frac{(\text{CKRas}(i) - 0.42)^2}{0.42^2} + \frac{(\text{ANKRas}(i) - 7)^2}{7^2}\right], \quad (12)$$

where CKRas(i) and ANKRas(i) are the simulated fraction of clustered K-Ras and averaged number of K-Ras/nanocluster, respectively, when the K-Ras.GTP number is $i \times 10\%$ of the maximal number of K-Ras.GTP. To have biological relevance, the Ras nanocluster fraction must reach a steady state in <5 min; therefore, estimates that did not generate steady-state simulations by 5 min were discarded.

RESULTS

Calculation of collision rates

To develop the mathematical model, we needed to estimate realistic collision rates on the plasma membrane. Thus, we calculated the collision rate a_{20} using a fixed number of Ras-Gal3 complexes and different time lags, Δt, as described in Methods. To reduce the computational time, we set the number of Ras-Gal3 complexes to 10% of the maximal number of K-Ras.GTP molecules and reduced the simulation surface area proportionally. When the time lag is relatively large, the diffusion distance of a protein may be greater than the averaged distance between two proteins. Thus, there is a decreased probability of protein collision. To avoid missing any possible collision events, Δt should satisfy $\sqrt{D\Delta t} < r$, where D is the protein diffusion rate (1 $\mu m^2/s$) and r is the radius of a Ras-Gal3 complex (~1.6 nm). Fig. 2 *A* gives the calculated protein collision rates with time lags ranging from $\Delta t = 10^{-5}$ s to $\Delta t = 10^{-12}$ s. The calculated collision rate increased as the time lag decreased. When the time lag was below a threshold value, which is $\Delta t = 10^{-10}$ s, the calculated collision rate remains constant (Fig. 2 *A*). This threshold value is well below the value of $r/\sqrt{D}$. We used this time lag as a standard to calculate other collision rates, because the threshold value can also be applied to the random diffusion of K-Ras proteins (radius ~0.8 nm) and

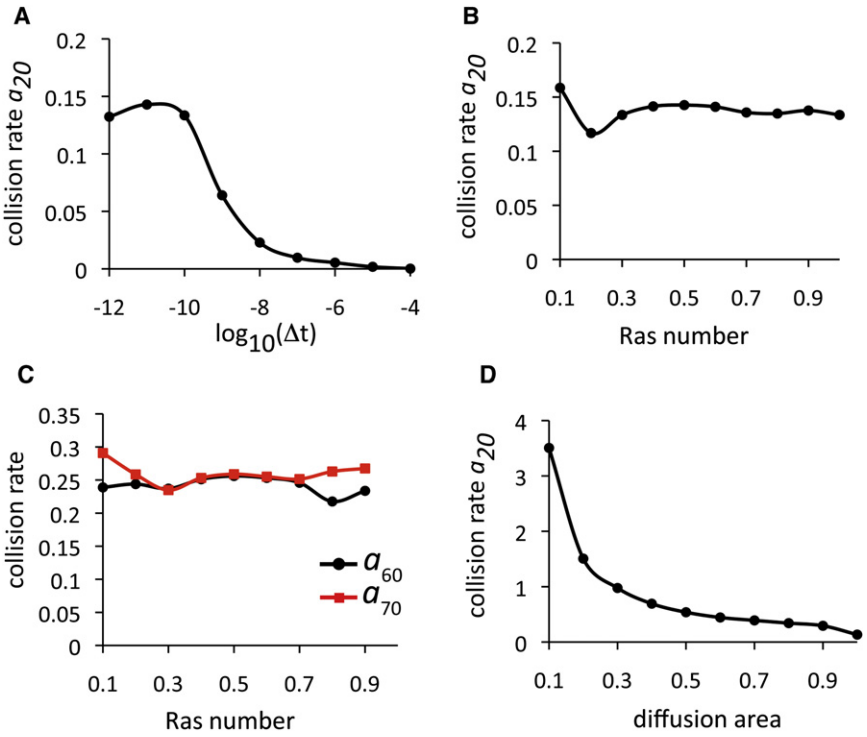

FIGURE 2 Computation of protein collision rates on the plasma membrane. (*A*) Collision rate (a_{20}/s) of Ras-Gal3 complexes calculated for different time lags. (*B*) Collision rate (a_{20}/s) of Ras-Gal3 complexes calculated for a fixed time lag, $\Delta t = 10^{-10}$ s and different numbers of K-Ras.GTP proteins on the plasma membrane. The maximal number of K-Ras.GTP on the plasma membrane is denoted as the unit 1. (*C*) Collision rates of Ras (a_{60}/s) and Ras-Gal3 complexes (a_{70}/s) with nanoclusters based on a fixed time lag, $\Delta t = 10^{-10}$ s, and different numbers of K-Ras.GTP proteins in nanoclusters on the plasma membrane. (*D*) Calculated collision rate (a_{20}/s) of Ras-Gal3 complexes if diffusion is restricted to a proportion of the diffusion area.

collisions with larger nanoclusters (radius ~9 nm). Our data show that collision rate a_{20} is independent of the numbers of Ras-Gal3 complexes and nanoclusters in the system (Fig. 2 *B*), as are the collision rates of K-Ras.GTP (a_{60}) and Ras-Gal3 complexes (a_{70}) with nanoclusters (Fig. 2 *C*). These results support our assumption that protein diffusion and collision occur in a homogeneous reaction system. When the system reaches the steady state via protein binding and disassociation reactions, this assumption may need to be reexamined. Since varying protein numbers had no significant impact on the collision rates, we used constant collision rates for all molecular numbers of K-Ras in the system.

We next tested the influence of cell surface area on the calculated collision rates. Results in Fig. 2, *A–C*, are based on a diffusion area equal to the area of the cell surface. Since K-Ras may diffuse on only a proportion of the cell surface if, for example, it is excluded from liquid-ordered nanodomains (7,8), we calculated the collision rates based on different proportions of the diffusion area. If the surface area is smaller, protein concentration will lead to larger collision rates. However, the change in collision rate is not significant unless the diffusion area decreases to <40% of the maximal area (Fig. 2 *D*). We therefore use rates obtained from the maximal diffusion area.

Estimation of model parameters

In the implementations of the genetic algorithm, we assumed that the initial estimates of the kinetic rates were uniformly distributed in the range $(0,W_{\max})$. To achieve a small estimation error, the value of $W_{\max}$ was determined by simulation. To find all of the possible values for the Gal3 number, we used a search range from zero to 5 times the maximal K-Ras.GTP number.

According to the Arrhenius equation, the protein binding reaction rate, a_i, can be represented by

$$a_i = a_{i0}\exp\left(\frac{E_{act}}{RT}\right), \quad i = 1 \sim 7, \tag{13}$$

where a_{i0} is the protein collision rate, E_{act} the activation energy, R the gas constant, and T the absolute temperature. Here, the value of the exponential function exp $(E_{\text{act}}/(KT))$ represents the probability of complex formation (*P*c). Based on the protein collision rates calculated in section Calculation of collision rates, the *P*c values of binding rates a_2, a_6, and a_7 were estimated by using the genetic algorithm. For simplicity, we assumed that the values of $a_2 \sim a_5$ are equal, since these reactions, up to and including pentamerization, involve the same molecular mechanism, i.e., oligomerization of Gal3. The *P*c values of these binding rates could, however, be slightly different.

Because of possible local maxima in the genetic algorithm, we selected the 10 best sets of estimated parameters that had the smallest estimation errors. The Gal3 numbers are presented in Fig. 3 *A* as the ratio of Gal3 number to the maximal number of K-Ras.GTP. The estimated ratio ranges from 0.43 to 0.71 and the averaged ratio is 0.5445. The best estimate of the Gal3 number with the minimal estimation error is ~56% of the maximal K-Ras.GTP number. The mean, standard deviation, and range of these 10 estimates are presented in Table 1. We used the set of parameters that generated the smallest estimation error as the final estimate, which is given in Fig. 3. The probabilities of a collision leading to complex formation are significantly different among the protein binding reactions. It is high during the assembly of a pentameric Ras-Gal3 nanocluster (*P*c = 0.0715 for $a_2 \sim a_5$) but is low for the incorporation of additional K-Ras proteins (*P*c = 9.96×10^{-5} for a_6) or Ras-Gal3 complexes (*P*c = 1.8×10^{-4} for a_7) into nanoclusters. We discuss the implications of this formulation later.

We next expanded the search area for each parameter from $(0,W_{\max})$ to $(0,kW_{\max})$ to determine whether this would further improve the accuracy of simulated nanocluster formation. Although it may be likely to find a set of kinetic rates with smaller estimation errors from a larger search space, the estimated kinetic rates from a larger search space may not be able to produce simulations with smaller estimation errors due to the possible local maxima in the genetic algorithm. We searched the model kinetic rates from search space $(0,kW_{\max})$ for every parameter, where $k = 1$, 2, 5, or 10. For each value of k, we obtained 20 sets of estimated parameters and found that the value of the minimal estimation error was in fact proportional to the value of k (results not shown). Therefore, we used the kinetic rates in Fig. 3 from search space $(0, W_{\max})$ as the final estimated parameters.

Simulated dynamics of nanocluster formation

Fig. 3 shows clustering data and simulated system dynamics using the best estimates of the model parameters. Fig. 3, *B* and *C*, shows the simulated fractions of K-Ras.GTP in nanoclusters and the average K-Ras number/nanocluster, respectively. At equilibrium, which was achieved after ~2 min of simulation time, the simulation successfully realized the observed experimental results with ~42% of K-Ras.GTP proteins in nanoclusters (8). Furthermore, the simulation returned the average number of Ras proteins/nanocluster as ~7, a result that again matches experimental data (8). The distribution histogram of the number of nanoclusters with different numbers of K-Ras.GTP in Fig. 3 *D* shows that the number of K-Ras.GTP in complexes with two, three, or four Ras proteins is ~2.1% of the total K-Ras proteins on the plasma membrane. Fig. 3 *D* also shows that the number of nanoclusters with five or more Ras proteins is inversely proportional to the number of Ras proteins in the nanocluster. Thus, the number of nanoclusters with 10 Ras proteins is~43% of the number of nanoclusters with five Ras proteins, these data lend support to our simplifying assumption of excluding nanoclusters with >10 Ras proteins

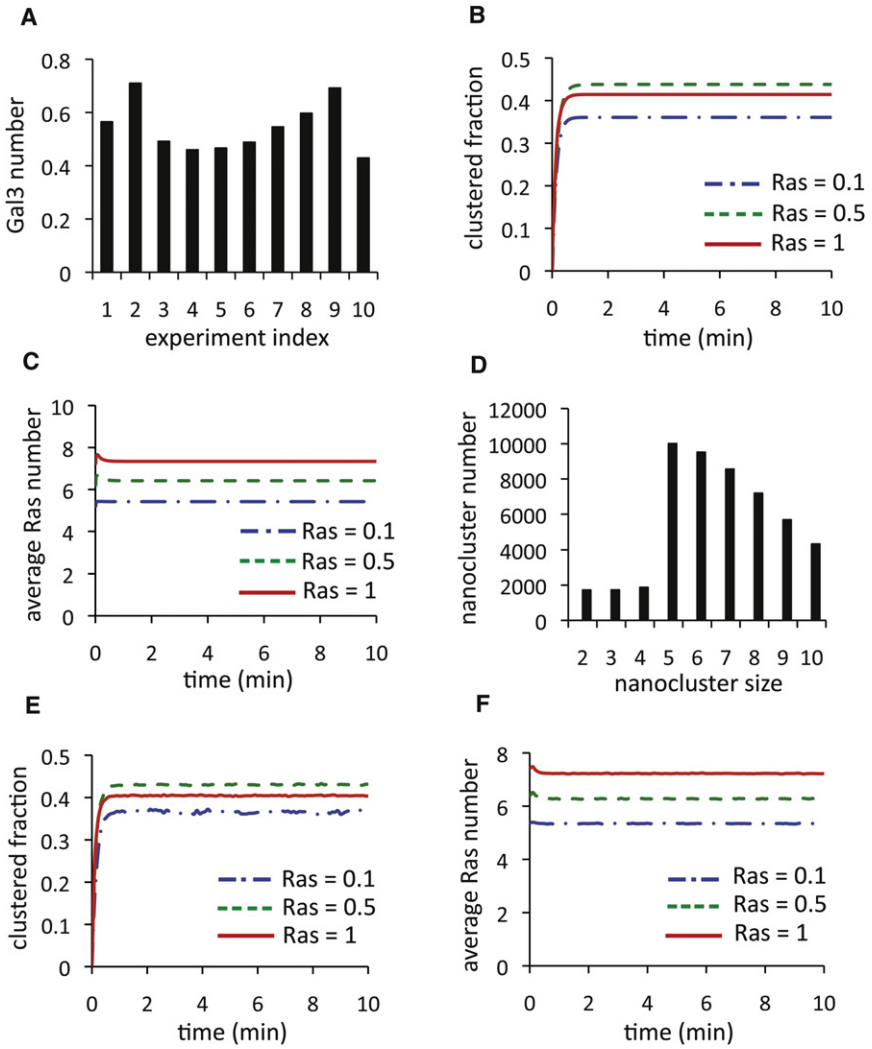

FIGURE 3 Estimated Gal3 numbers and simulated nanocluster formation dynamics. (*A*) Estimated Gal3 numbers in 10 sets of model parameters using the genetic algorithm. The Gal3 numbers are presented as the ratio of Gal3 to Ras. (*B*) Simulation results of K-Ras nanocluster formation showing the progression of the system to equilibrium. We simulated the complete model shown in Fig. 1 for 5 min of real time with the following estimated kinetic rates: $a_1 = 1.2786 \times 10^{-7}/\ s$, $d_1 = 0.0595/\ s$, $a_2 = 0.0101/$ s, $d_2 = 0.9483/\ s$, $a_6 = 2.4791 \times 10^{-5}/\ s$, $a_7 = 4.7839 \times 10^{-4}/\ s$, $d_6 = 2.5/\ s$, $d_7 = 2.5/\ s$, $d_8 = 2.5/\ s$, $d_9 = 0.0999/\ s$, and $d_{10} = 0.0596/\ s$. The nonzero initial conditions are [Ras] = 774,000, [Gal3] = 43,730. (*C*) Average K-Ras.GTP number in each nanocluster during the course of the simulation. (*D*) Distribution of nanoclusters with different numbers of K-Ras.GTP proteins. (*E*) Stochastic simulation results of K-Ras nanocluster formation showing the progression of the system to equilibrium. We simulated biochemical reactions 1–10 (see Methods) for 5 min of real time with the same kinetic rates as in *B*. (*F*) Average K-Ras.GTP number in each nanocluster during the course of the simulation.

from the model. The ability of the model to equilibrate by 2 min of simulation is an important result, because Ras.GTP loading in response to acute growth factor stimulation also occurs on this timescale (5).

To further validate the deterministic model, a stochastic model based on the same 136 reactions (Eqs. 1–10) was also developed and we used the stochastic simulation algorithm to simulate the biochemical reactions (Eqs. 1–10) directly. The stochastic simulation results (Fig. 3, *E* and *F*) show only slight fluctuations in the simulated clustered fractions and average numbers of K-Ras.GTP/nanocluster. The simulations in Fig. 3 therefore support the use of a deterministic model to simulate stochastic protein diffusion and collision when the K-Ras.GTP number is large.

The number of Gal3 molecules determines the fraction of K-Ras.GTP in nanoclusters

To test the importance of the number of Gal3 molecules available for recruitment, we simulated the system dynamics

TABLE 1 Mean and standard deviation (SD) of the 10 sets of estimated model parameters

	a_1	d_1	a_2	d_2	a_6
Mean	7.505E-8/*s*	0.0384/*s*	8.027E-3/*s*	0.9501/*s*	2.928E-5/*s*
SD	2.991E-8	0.0131	4.853E-3	0.0467	4.741E-6
Range	(4.07E-8,1.36E-7)	(0.020,0.060)	(3.36E-3,0.02)	(0.872,0.997)	(1.27E-5,3.92E-5)
	a_7	d_9	d_{10}	Gal3	
Mean	5.305E-4/s	0.0994/s	0.0538/s	0.5443	
SD	7.960E-7	6.494E-4	0.0121	0.0968	
Range	(5.27E-4,5.31E-4)	(0.098,0.1)	(0.034,0.0791)	(0.429,0.710)	

The Gal3 number is the product of 774,000 and the value in this table.
The value d_8 (2.5/s) is determined by experiments. The values of d_6 and d_7 are assumed to be equal to that of d_8.

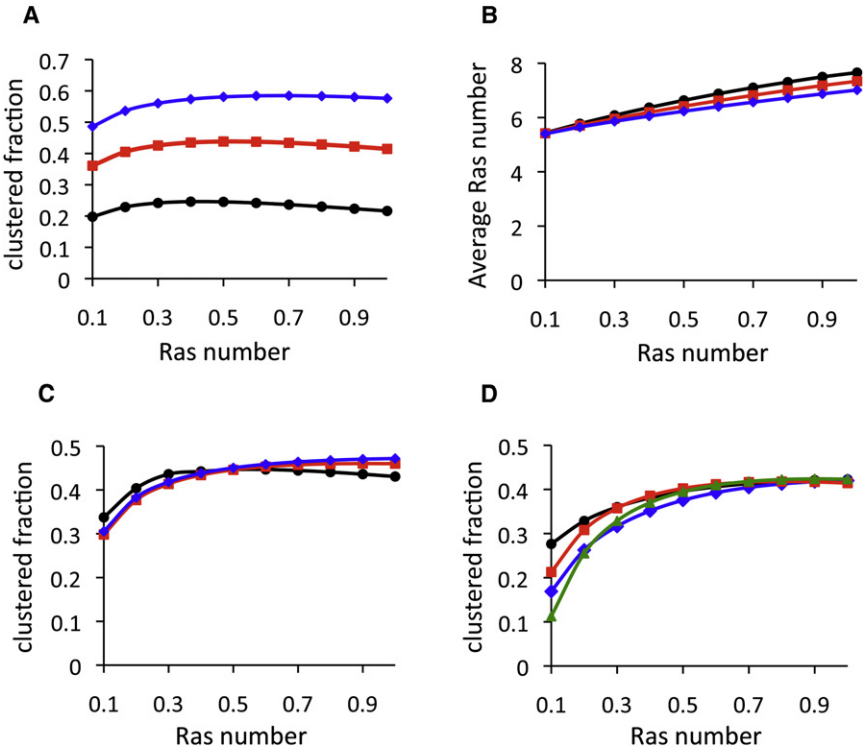

FIGURE 4 The Gal3 number determines nanocluster formation. (*A*) Fraction of K-Ras.GTP in nanoclusters with different numbers of Gal3 in the cytosol. The model was simulated for 5 min of real time with Gal3/K-Ras.GTP ratios of 0.25, 0.565, and 1 (*circles*, ratio = 0.25; *squares*, ratio = 0.565; *diamonds*, ratio = 1). (*B*) Average K-Ras number/nanocluster with different numbers of Gal3 in the cytosol (*circles*, Gal3/K-Ras.GTP ratio = 0.25; *squares*, ratio = 0.565; *diamonds*, ratio = 1). (*C*) Fraction of K-Ras.GTP in nanoclusters assuming a fixed Gal3 number in the cytosol and estimating other modeling parameters based on the assumed Gal3 number (*circles*, Gal3 = 0.565 × (max K-Ras number) and all the other rates as presented in Fig. 2; *squares*, Gal3 = (max K-Ras number); *diamonds*, Gal3 = 2 × (max K-Ras number); *triangles*, Gal3 = 5 × (max K-Ras number)). (*D*) Clustered fraction of K-Ras when Gal3 number equals the maximal number of K-Ras.GTP. In each case shown, one of the kinetic rates was changed to realize the experimental result that ~42% of K-Ras molecules are in nanoclusters when the K-Ras number is maximal (*circles*, $a_1 = a_1 / 2.8$; *squares*, $d_1 = d_1 \times 1.25$; *diamonds*, $a_2 = a_2 / 28$; *triangles*, $d_2 = d_2 \times 700$). In all four figures, the maximal number of K-Ras.GTP on the plasma membrane is denoted as the unit 1.

with different numbers of Gal3 and K-Ras.GTP proteins. The results in Fig. 4 *A* show that for each expression level of Gal3 the fraction of K-Ras.GTP in nanoclusters remains constant over the complete range of K-Ras.GTP protein numbers tested. This is an important result, because the model successfully realizes a constant fraction of K-Ras.GTP proteins in nanoclusters over a wide range of K-Ras.GTP expression levels, as observed in intact cells (8). Fig. 4 *A* also shows that the fraction of K-Ras proteins in nanoclusters is directly proportional to the number of Gal3 molecules available for recruitment. When the number of Gal3 molecules available for recruitment is equal to ~56% of the maximal number of K-Ras.GTP on the plasma membrane, the fraction of K-Ras.GTP in nanoclusters is always ~42% (Fig. 3 *A*). If the Gal3 levels are lower or higher, the clustered fraction is reset accordingly, but remains constant against K-Ras.GTP levels. The simulation results also suggest that the average number of K-Ras.GTP/nanocluster is weakly dependent on the number of K-Ras.GTP proteins on the plasma membrane. If the number of K-Ras.GTP on the plasma membrane is low (~10% of the maximal number), then the majority of nanoclusters are pentamers (Fig. 4 *B*). The results shown in Fig. 4 indicate that the clustered fraction of K-Ras.GTP is determined by the cytosolic concentration of Gal3. Our previous cell biological experiments revealed that the level of K-Ras.GTP clustering increased in proportion to increased Gal3 expression levels (13). The simulations of the mathematical model are fully consistent with these biological results.

To explore in more detail the relationship between the numbers of Gal3 and K-ras.GTP in the model with the maintenance of a fixed clustered fraction, we conducted two further experiments. First, given that the number of Gal3 molecules in the model system is close to the number of K-Ras.GTP in nanoclusters, we asked whether or not we could realize a constant fraction of 42% K-Ras.GTP in nanoclusters with a much larger Gal3 number. We set the Gal3 number to be equal to, or 2 times or 5 times, the maximal K-Ras.GTP number. For each Gal3 number the genetic algorithm was used to search for new values of eight model kinetic rates (a_1, d_1, a_2, d_2, a_6, a_7, d_9, and d_{10}) that provided the closest fit to our experimental data. The simulated clustered fractions based on these different assumed Gal3 numbers are presented in Fig. 4 *C*. In all three tests, the clustered fractions showed a much greater dependence on K-Ras.GTP numbers than that shown in Fig. 4 *A*.

Second, we modified the system so that the number of Gal3 molecules in the cytosol for recruitment was equal to the maximal number of K-Ras.GTP molecules on the plasma membrane. We then adjusted each of the four kinetic rates a_1, d_1, a_2, and d_2 to realize the observed value of 42% of K-Ras.GTP in nanoclusters for the maximal number of K-Ras.GTP proteins. However, in direct contrast to our experimental results, these simulation results indicated that for each of these four kinetic rates the simulated fraction of K-Ras.GTP in nanoclusters was always dependent on the number of K-Ras.GTP proteins (Fig. 4 *D*). Since any change in one of these four parameters generated a similar decreasing pattern for the percentage of K-Ras.GTP

in nanoclusters, any combination of changes in these four parameters will generate results similar to those presented in Fig. 4 *D*. In sum, these results illustrate that the number of Gal3 proteins in the cytosol available for recruitment is a key parameter that determines the fraction of K-Ras.GTP in nanoclusters.

Rapid formation of Ras-Gal3 pentamers

The estimated rate of Ras-Gal3 pentamer formation (a_2 = 0.0101/ s) presented in Fig. 3 is much larger than the rate of a Ras-Gal3 complex binding to nanoclusters (a_7 = 4.7839×10^{-4}/s). To explore the relevance of the fast formation of Ras-Gal3 pentamers to K-Ras nanoclustering, we tested the possibility of having a smaller binding rate, a_2. We set the value of a_2 to be 0.001/s, 0.0001/s, and 0.00001/s, respectively, and used the genetic algorithm to search the other seven kinetic rates together with the Gal3 number based on each assumed value of a_2. The simulation results in Fig. 5 indicate that the system cannot generate the constant fractions of K-Ras in nanoclusters if the value of a_2 is very small. When the value of a_2 is 0.00001/s, which is close to a_7 in Fig. 2, simulated clustered fractions are much smaller than the experimentally observed value (~42%). Simulation results in Fig. 4 are consistent with experimental observations that the conversion of Gal3 from monomer to pentamer is fast (11) and suggest that the fast formation of Gal3 pentamers is a second key feature of the mechanism for delivering a constant fraction of K-Ras.GTP molecules in nanoclusters. These estimated rates also validate our initial assumption to exclude the weak binding of K-Ras.GTP to Ras-Gal3 complexes in the formation of dimeric, trimeric, or tetrameric (Ras)*i*-(Ras-Gal)*j* complexes by random diffusion.

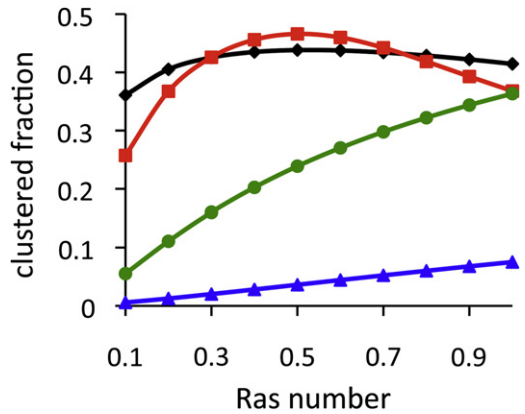

FIGURE 5 Nanocluster formation for different values of binding rate a_2. Fraction of K-Ras.GTP in nanoclusters assuming a fixed value of binding rate a_2 and estimating other kinetic rates and Gal3 number based on the assumed value of a_2: *diamonds*, a_2 = 0.0101 / *s*; *squares*, a_2 = 0.001 / *s*; *circles*, a_2 = 0.0001 / *s*; *triangles*, a_2 = 0.00001 / *s*. The maximal number of K-Ras.GTP on the plasma membrane is denoted as the unit 1.

Robustness of the model

We evaluated the robustness properties of the proposed model by testing the effect on the system dynamics of varying one of the eight estimated reaction rates (a_1, d_1, a_2, d_2, a_6, a_7, d_9, and d_{10}). For each set of reaction rates, we determined the fraction of K-Ras.GTP in nanoclusters and the average number of K-Ras.GTP proteins/nanocluster for different K-Ras.GTP numbers. The clustered fraction is sensitive to changes in kinetic rates a_1, d_1, a_2, d_9, or d_{10}, but is robust to changes of the other kinetic rates, d_2, a_6, or a_7 (Fig. S1 in the Supporting Material). The fraction of K-Ras.GTP in nanoclusters is also robust to changes in K-Ras.GTP number for different values of the six reaction rates (a_1, d_1, a_2, d_2, a_6, and a_7). We also show that variation of kinetic rates a_1, d_1, a_2, d_2, d_9, or d_{10} has no significant influence on the average number of K-Ras.GTP proteins/nanocluster (Fig. S2). Increasing or decreasing a_6 or a_7, however, affects the number of K-Ras molecules/nanocluster (Fig. S2). In summary, the simulation results in Fig. S1 show that the model is robust to changes of K-Ras.GTP numbers under a variety of different system conditions.

DISCUSSION

The formation of K-Ras nanoclusters, which function as transient nanoscale digital switches in MAPK activation, is essential for Ras signal transduction (5). How K-Ras.GTP nanoclusters form and what mechanism operates to maintain the K-Ras clustered fraction at a constant level over a wide range of K-Ras.GTP concentrations is unresolved. We tackle this problem here using in silico modeling to show that interactions between K-Ras and a cytosolic pool of Gal3 play a central role in driving K-Ras nanoclustering on the plasma membrane. We developed a mathematical model to simulate the dynamics of K-Ras nanoclustering on the plasma membrane. We applied a genetic algorithm to search the possible model parameters capable of realizing the experimental observations and to validate the optimal estimated parameters representing the collision mechanisms. In addition, a computational method was designed to calculate protein collision rates based on experimentally determined protein diffusion rates and diffusion mechanisms. Calculated collision rates were constant over a wide range of protein numbers, supporting our use of a homogeneous reaction system to describe the two-dimensional Ras protein diffusion on the plasma membrane. The model successfully realizes the constant fraction of clustered Ras based on the known biochemistry of Gal3 and, it is important to note, predicts that a key mechanism for this constant fraction is the availability of Gal3 protein in the cytosol for recruitment to the plasma membrane. Furthermore, our simulations demonstrate that the probability of protein complex formation is a useful parameter to use in combination with constant collision rates to define binding rates that realize experimental data.

Based on our published results of quantitative EM and FLIM-FRET imaging (13), the in silico model proposes that Gal3 proteins are recruited to the plasma membrane as a result of molecular collisions with freely diffusing K-Ras.GTP monomers. The resulting K-Ras.GTP-Gal3 complexes rapidly assemble into pentameric complexes driven by molecular interactions between the constituent Gal3 proteins. Pentameric nanoclusters may accumulate additional K-Ras.GTP or K-Ras.GTP-Gal3 complexes. However, our simulations show that the probability of successful incorporation of additional K-Ras proteins after collision with a K-Ras.Gal3 pentamer must be much lower than during the assembly of the pentamer, perhaps reflecting a different biophysical retention mechanism. One possibility is that the relatively stable complex of five K-Ras proteins anchored to the membrane by polybasic domains and a Gal3 pentamer remodels the nanoscale lipid environment of the cluster. By analogy with myristoylated alanine-rich C kinase substrate binding to the plasma membrane (36), remodeling would involve an increase in the local concentration of acidic phospholipids including PS and PIP_2, allowing further recruitment of positively charged K-Ras proteins, but with a lower affinity than that realized by direct Gal3 protein-protein interaction.

Whatever the precise mechanism, the model we have formulated faithfully delivers the important result of concentration-independent K-Ras.GTP nanocluster formation with the previously observed K-Ras stoichiometry and nanocluster lifetime (8–10). The model also recapitulates our recently published experimental results showing that the availability of Gal3 in the cytosol is the critical determinant of the K-Ras.GTP clustered fraction (13). Thus, altering the expression of Gal3 directly modulates signal transmission via K-Ras (14,37). These findings are significant because Gal3 expression and its subcellular localization are altered in a number of tumor types (38). Given that the clustered fraction is a critical determinant of the sensitivity of a cell to EGF-dependent activation of the MAPK cascade (5), the new data implicate the cytosolic pool of Gal3 as a modulator of MAPK activation by EGF as well as signal output from oncogenic mutant K-RasG12V. Taken together, these data implicate altered Gal3 expression in K-Ras-mediated tumorigenesis.

For an ordinary differential equation system having steady-state solutions, the kinetic rates in the model should be constrained by the equilibrium conditions of the system. However, our simulations suggest that this system may not be fully balanced; for example, when we changed the values of pairs of parameters, such as a_1 and d_1, simultaneously and proportionally, the equilibrium properties of the system were altered. In addition, the simulated distributions of nanocluster size neither became exponential nor had a large aggregate whose size scaled with the total number of molecules. These observations suggest that nanocluster formation is regulated by certain key nonquilibrium processes. Indeed, the system includes a number of unidirectional reactions, such as the disassembly of nanoclusters and the separation of Ras-Gal3 complexes within nanoclusters. In addition the fast formation of Gal3 pentamers results in very different binding rates for Ras-Gal3 pentamer assembly versus nanocluster growth as a result of additional Ras and Ras-Gal3 collisions. A more detailed analysis of the interaction between balanced and unbalanced reactions via the steady-state solutions would be interesting to pursue. However, this is not a trivial exercise, because our modeled system includes 27 equations and the equations involving K-Ras.GTP, Gal3, and Ras-Gal3 species are complex. In the future, other theoretical approaches, such as the master equation method, could be used to analyze nanocluster kinetics and give deeper insights into the underlying physics of nanocluster formation.

A number of lipid-anchored proteins have been shown to operate in distinct nanoclusters on the inner and outer leaflets of the plasma membrane, including other Ras isoforms and GPI-anchored proteins (7–9,39,40). All of these proteins show a concentration-independent clustered fraction and an excess of monomer over clustered protein, albeit with different numbers of protein in each nanocluster. Although the model we have developed is specific to K-Ras nanoclustering, at the core of the model is a mechanism that rapidly promotes cooperative interaction between monomers and dimers. For K-Ras, this cooperativity is provided by protein-protein binding. In attempting to generalize the model, we speculate that a similar core mechanism might operate for other nanoclustered proteins, perhaps driven by protein-protein or protein-lipid interactions. Such a hypothesis is readily tractable by simulation and experiment and may allow the definition of a common biophysical principle for the nonrandom organization of lipid-anchored proteins on the plasma membrane.

SUPPORTING MATERIAL

Mathematical model of differential equations, simulation method of the stochastic model, and two figures are available at http://www.biophysj.org/biophysj/supplemental/S0006-3495(10)00553-9.

Y.K. is the incumbent of The Jack H. Skirball Chair for Applied Neurobiology. J.F.H. is the incumbent of the Fondren Chair in Cellular Signaling.

This work was supported by award No. R01GM066717 from the National Institute of General Medical Sciences to J.F.H. and by grants from the Australian Research Council and the United States-Israel Binational Science Foundation.

REFERENCES

1. Cox, A. D., and C. J. Der. 2003. The dark side of Ras: regulation of apoptosis. *Oncogene*. 22:8999–9006.
2. Downward, J. 2003. Targeting RAS signalling pathways in cancer therapy. *Nat. Rev. Cancer*. 3:11–22.
3. Huang, C. Y., and J. E. Ferrell, Jr. 1996. Ultrasensitivity in the mitogen-activated protein kinase cascade. *Proc. Natl. Acad. Sci. USA*. 93: 10078–10083.

4. Bhalla, U. S., P. T. Ram, and R. Iyengar. 2002. MAP kinase phosphatase as a locus of flexibility in a mitogen-activated protein kinase signaling network. *Science.* 297:1018–1023.
5. Tian, T., A. Harding, …, J. F. Hancock. 2007. Plasma membrane nanoswitches generate high-fidelity Ras signal transduction. *Nat. Cell Biol.* 9:905–914.
6. Breitling, R., and D. Hoeller. 2005. Current challenges in quantitative modeling of epidermal growth factor signaling. *FEBS Lett.* 579: 6289–6294.
7. Prior, I. A., C. Muncke, …, J. F. Hancock. 2003. Direct visualization of Ras proteins in spatially distinct cell surface microdomains. *J. Cell Biol.* 160:165–170.
8. Plowman, S. J., C. Muncke, …, J. F. Hancock. 2005. H-ras, K-ras, and inner plasma membrane raft proteins operate in nanoclusters with differential dependence on the actin cytoskeleton. *Proc. Natl. Acad. Sci. USA.* 102:15500–15505.
9. Hancock, J. F., and R. G. Parton. 2005. Ras plasma membrane signalling platforms. *Biochem. J.* 389:1–11.
10. Murakoshi, H., R. Iino, …, A. Kusumi. 2004. Single-molecule imaging analysis of Ras activation in living cells. *Proc. Natl. Acad. Sci. USA.* 101:7317–7322.
11. Plowman, S. J., N. Ariotti, …, J. F. Hancock. 2008. Electrostatic interactions positively regulate K-Ras nanocluster formation and function. *Mol. Cell. Biol.* 28:4377–4385.
12. Harding, A. S., and J. F. Hancock. 2008. Using plasma membrane nanoclusters to build better signaling circuits. *Trends Cell Biol.* 18:364–371.
13. Shalom-Feuerstein, R., S. J. Plowman, …, Y. Kloog. 2008. K-ras nanoclustering is subverted by overexpression of the scaffold protein galectin-3. *Cancer Res.* 68:6608–6616.
14. Elad-Sfadia, G., R. Haklai, …, Y. Kloog. 2004. Galectin-3 augments K-Ras activation and triggers a Ras signal that attenuates ERK but not phosphoinositide 3-kinase activity. *J. Biol. Chem.* 279: 34922–34930.
15. Dumic, J., S. Dabelic, and M. Flögel. 2006. Galectin-3: an open-ended story. *Biochim. Biophys. Acta.* 1760:616–635.
16. Mehul, B., S. Bawumia, and R. C. Hughes. 1995. Cross-linking of galectin 3, a galactose-binding protein of mammalian cells, by tissue-type transglutaminase. *FEBS Lett.* 360:160–164.
17. Ahmad, N., H. J. Gabius, …, C. F. Brewer. 2004. Galectin-3 precipitates as a pentamer with synthetic multivalent carbohydrates and forms heterogeneous cross-linked complexes. *J. Biol. Chem.* 279:10841–10847.
18. Chen, I. J., H. L. Chen, and M. Demetriou. 2007. Lateral compartmentalization of T cell receptor versus CD45 by galectin-N-glycan binding and microfilaments coordinate basal and activation signaling. *J. Biol. Chem.* 282:35361–35372.
19. Lajoie, P., E. A. Partridge, …, I. R. Nabi. 2007. Plasma membrane domain organization regulates EGFR signaling in tumor cells. *J. Cell Biol.* 179:341–356.
20. Nieminen, J., A. Kuno, …, S. Sato. 2007. Visualization of galectin-3 oligomerization on the surface of neutrophils and endothelial cells using fluorescence resonance energy transfer. *J. Biol. Chem.* 282:1374–1383.
21. Burrage, K., J. Hancock, …, D. V. Nicolau, Jr. 2007. Modelling and simulation techniques for membrane biology. *Brief. Bioinform.* 8:234–244.
22. Batada, N. N., L. A. Shepp, and D. O. Siegmund. 2004. Stochastic model of protein-protein interaction: why signaling proteins need to be colocalized. *Proc. Natl. Acad. Sci. USA.* 101:6445–6449.
23. Lommerse, P. H., B. E. Snaar-Jagalska, …, T. Schmidt. 2005. Single-molecule diffusion measurements of H-Ras at the plasma membrane of live cells reveal microdomain localization upon activation. *J. Cell Sci.* 118:1799–1809.
24. Lommerse, P. H., K. Vastenhoud, …, T. Schmidt. 2006. Single-molecule diffusion reveals similar mobility for the Lck, H-ras, and K-ras membrane anchors. *Biophys. J.* 91:1090–1097.
25. Saffman, P. G., and M. Delbrück. 1975. Brownian motion in biological membranes. *Proc. Natl. Acad. Sci. USA.* 72:3111–3113.
26. Nicolau, Jr., D. V., …, K. Burrage, J. F. Hancock. 2006. Identifying optimal lipid raft characteristics required to promote nanoscale protein-protein interactions on the plasma membrane. *Mol. Cell. Biol.* 26:313–323.
27. Nicolau, Jr., D. V., J. F. Hancock, and K. Burrage. 2007. Sources of anomalous diffusion on cell membranes: a Monte Carlo study. *Biophys. J.* 92:1975–1987.
28. Mayawala, K., D. G. Vlachos, and J. S. Edwards. 2006. Spatial modeling of dimerization reaction dynamics in the plasma membrane: Monte Carlo vs. continuum differential equations. *Biophys. Chem.* 121:194–208.
29. Turner, M. S., P. Sens, and N. D. Socci. 2005. Nonequilibrium raftlike membrane domains under continuous recycling. *Phys. Rev. Lett.* 95:168301.
30. Richardson, G., L. J. Cummings, …, P. O'Shea. 2007. Toward a mathematical model of the assembly and disassembly of membrane microdomains: comparison with experimental models. *Biophys. J.* 92:4145–4156.
31. Gregory, S. M., A. Cavenaugh, …, P. F. Almeida. 2008. A quantitative model for the all-or-none permeabilization of phospholipid vesicles by the antimicrobial peptide cecropin A. *Biophys. J.* 94:1667–1680.
32. Niv, H., O. Gutman, …, Y. I. Henis. 2002. Activated K-Ras and H-Ras display different interactions with saturable nonraft sites at the surface of live cells. *J. Cell Biol.* 157:865–872.
33. Almeida, P. F. F., and W. L. C. Vaz. 1995. Structure and dynamics of membranes. *In* From Cells to Vesicles. R. Lipowsky and E. Sackmann, editors. Elsevier. 305–357.
34. Chipperfield, A. J., Fleming, P.J., and Pohlheim, H. 1994. A Genetic Algorithm Toolbox for MATLAB. *Proc. Int. Conf. Sys. Eng., Coventry, UK.* 200–207.
35. Kurata, H., K. Masaki, …, R. Iwasaki. 2005. CADLIVE dynamic simulator: direct link of biochemical networks to dynamic models. *Genome Res.* 15:590–600.
36. Wang, J., A. Gambhir, …, S. McLaughlin. 2002. Lateral sequestration of phosphatidylinositol 4,5-bisphosphate by the basic effector domain of myristoylated alanine-rich C kinase substrate is due to nonspecific electrostatic interactions. *J. Biol. Chem.* 277:34401–34412.
37. Shalom-Feuerstein, R., T. Cooks, …, Y. Kloog. 2005. Galectin-3 regulates a molecular switch from N-Ras to K-Ras usage in human breast carcinoma cells. *Cancer Res.* 65:7292–7300.
38. Califice, S., V. Castronovo, and F. Van Den Brûle. 2004. Galectin-3 and cancer (Review). *Int. J. Oncol.* 25:983–992, (Review).
39. Sharma, P., R. Varma, …, S. Mayor. 2004. Nanoscale organization of multiple GPI-anchored proteins in living cell membranes. *Cell.* 116:577–589.
40. Hancock, J. F. 2006. Lipid rafts: contentious only from simplistic standpoints. *Nat. Rev. Mol. Cell Biol.* 7:456–462.